

Exact Thermodynamic Analysis of a Hybrid Molecular Motor Switching Between Active and Passive Modes

Mesfin Asfaw Taye

*West Los Angeles College, Science Division
9000 Overland Ave, Culver City, CA 90230, USA**

We present an exact analytical study of a hybrid molecular motor that operates under a combination of active and passive transport modes. Rather than modeling an explicit time-dependent switching process, we analyze the system in terms of a steady-state hybrid regime that interpolates between purely passive and active limits. In the quasistatic limit, when the ratchet potential is switched off, the system effectively functions as a chemically driven active motor and its efficiency asymptotically approaches unity, which is the theoretical upper bound for such autonomous machines. On the other hand, when a spatially periodic ratchet potential is coupled with a nonuniform temperature field, the motor may operate as a passive Brownian heat engine depending on the parameter choice. Thus, its efficiency in the quasistatic regime converges to the Carnot efficiency in the absence of self-propulsion velocity. In intermediate regions (where both the passive and active forces contribute), the motor's efficiency ranges from the Carnot efficiency to one at the quasistatic limit. These findings not only present the distinct thermodynamic boundaries for active and passive transport but also give us fundamental insights into how energy conversion efficiency is shaped by the interplay of self-propulsion, external potentials, and thermal asymmetry in microscale systems.

PACS numbers:

Keywords: Brownian heat engine; stochastic thermodynamics; Langevin dynamics; entropy production; efficiency at maximum power.

I. INTRODUCTION

Studying noise-induced transport in microscale systems is vital for a basic understanding of nonequilibrium statistical physics [1, 2] because it has applications in microfluidics, biological transport, and energy conversion. Some of the most important questions worth asking in this context include: What happens when a chemically powered motor enters a spatially varying thermal landscape? In hybrid systems, directed motion emerges from two competing sources: internal activity and environmental asymmetry. This leads to new questions regarding efficiency and control at the microscale. Can a nanoscale machine combine the self-propulsion of active matter with thermal rectification to exceed the classical efficiency bounds?

Earlier, several studies have shown that directed motion can occur when Brownian particles interact with periodic potentials and broken spatiotemporal symmetries [3–12]. In their pioneering studies, Reimann et al. *et al.* [13] explored current generation via flashing and rocking ratchets, whereas recent work has focused on thermodynamic performance in spatially varying temperature fields [14–28]. Based on previous results [22], we also analyzed a Brownian motor operating in a ratchet potential

with an exponentially decreasing temperature profile and temperature-dependent viscous friction [29, 30] which is relevant because the setup mimics localized heating and enables high-efficiency thermal control at small scales. Recently, due to their technological relevance, the physics of active Brownian motors has garnered considerable attention. See, for example, recent works [31–40].

Although the thermodynamics of active and passive Brownian motors have been studied separately, less is known about systems that combine both behaviors. In particular, it is not known how a system that simultaneously incorporates self-propulsion and thermal rectification behaves thermodynamically. In earlier works, such as the study published in EPJB [14], the analysis focused exclusively on passive Brownian motors operating in ratchet potentials under thermal asymmetry without any active component. In contrast, when an active motor or nanoscale robot moves autonomously in one direction and interacts with both the ratchet potential and the spatially varying temperature field, it operates as a hybrid motor. This system exhibits two distinct sources of directed motion: self-propulsion due to internal energy conversion and rectification from the asymmetric ratchet potential coupled with the temperature gradient. A key question arises: How does the efficiency of such a hybrid

motor behave, particularly in the quasistatic limit, where thermodynamic reversibility may be approached?

While the active matter in a thermal bath can exceed the Carnot efficiency, once coupled to a thermal environment, its efficiency is limited by thermal asymmetry and active forces. Active Brownian motors can achieve unity efficiency under ideal conditions [41–43]. However, when subjected to a thermal bath with a temperature gradient, their efficiency is also constrained by the Carnot limit, $\eta_{\text{Carnot}} = 1 - \frac{T_c}{T_h}$, in the absence of self-propulsion velocity. Thus, while active motors may surpass the Carnot efficiency in some cases, thermal dissipation imposes fundamental efficiency limits.

In this work, we consider a simple hybrid molecular motor that combines active and passive transport modes. Rather than explicitly modeling a time-dependent switching process, we examine the system under a steady-state regime that interpolates between purely active and purely passive dynamics. This formulation captures the essential physics of systems in which self-propulsion and thermal ratcheting mechanisms coexist. We find that in the quasistatic limit, when the ratchet potential is switched off, the system effectively behaves as a chemically driven active motor, and its efficiency asymptotically approaches unity, which is the maximal efficiency achievable for such autonomous machines. In contrast, when both ratchet potential and thermal asymmetry are present, the motor behaves as a passive Brownian heat engine and, remarkably, achieves the Carnot efficiency $\eta = 1 - \frac{T_c}{T_h}$ in the absence of self-propulsion velocity, which sets the fundamental upper bound for any thermodynamic engine operating between the two heat reservoirs. In the intermediate regions (where both the passive and active forces contribute), the motor efficiency ranges between the Carnot efficiency and one, which indicates the dual contribution of thermal rectification and self-propulsion. This behavior demonstrates the transition from purely passive to hybrid active-passive operation, with efficiencies ranging from the fundamental thermodynamic limit of Carnot to the idealized efficiency of a chemically driven engine.

Our analysis shows that both the asymmetry of the temperature profile and the presence of an external load control the magnitude and direction of the particle current. The motor's velocity can be tuned by adjusting the potential barrier height, thermal noise intensity, and load, enabling transitions between the heat engine and refrigerator modes. We further examine key thermodynamic quantities—such as entropy, entropy production, and entropy extractions.

In this section, we discuss the non-equilibrium thermodynamic properties of a Brownian particle that moves under the influence of the potential $U(x) = U_s(x) + (f - \gamma v_0)x$, where f is the external load and $U_s(x)$ denotes a periodic ratchet potential [16]. To study the case of an active motor, we replace f with an effective force $f - \gamma v_0$, where v_0 is the constant active propulsion velocity. From this point onward, we set $\gamma = 1$ for simplicity. The

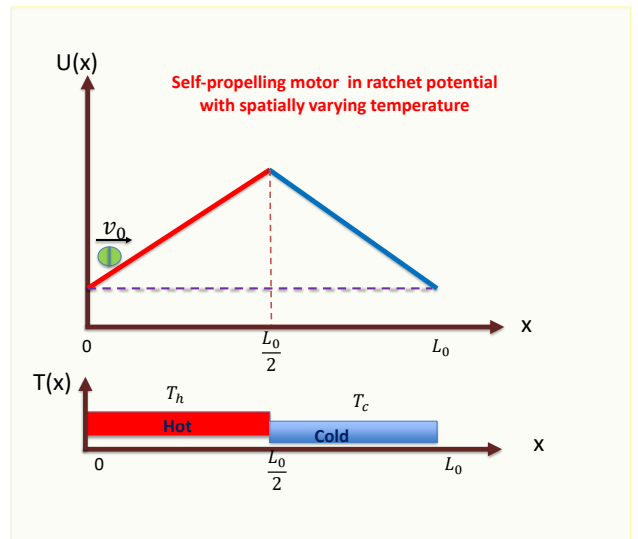


FIG. 1: (Color online) Schematic diagram for a Brownian particle in a piecewise linear potential in the absence of external load.

ratchet potential is defined as

$$U_s(x) = \begin{cases} 2U_0[\frac{x}{L_0}], & \text{if } 0 < x \leq L_0/2; \\ 2U_0[\frac{L_0-x}{L_0} + 1] & \text{if } L_0/2 < x \leq L_0; \end{cases} \quad (1)$$

which is spatially periodic, such that $U_s(x + L_0) = U_s(x)$ (see Fig. 1), with potential maxima at $x = L_0/2$ and minima at $x = 0$ and $x = L_0$. The background temperature is a piecewise constant:

$$T(x) = \begin{cases} T_h, & \text{if } 0 \leq x \leq \frac{L_0}{2}; \\ T_c, & \text{if } \frac{L_0}{2} \leq x \leq L_0. \end{cases} \quad (2)$$

Here, U_0 and L_0 represent the barrier height and the spatial period of the ratchet potential, respectively. Hereafter, whenever we plot figures, we use dimensionless variables: load $\bar{f} = fL_0/T_c$, $\bar{v}_0 = v_0L_0/T_c$, temperature $\bar{T}(x) = T(x)/T_c$, potential height $\bar{U}_0 = U_0/T_c$, and position $\bar{x} = x/L_0$. We also define $\tau = T_h/T_c$ and $\beta = \gamma L_0^2/T_c$. Hereafter, we drop all bars and set $\beta = 1$.

In the overdamped regime, the particle dynamics are governed by the Smoluchowski equation:

$$\frac{\partial P(x,t)}{\partial t} = \frac{\partial}{\partial x} \left[(U'_s(x) + f - v_0) P(x,t) + T(x) \frac{\partial P(x,t)}{\partial x} \right], \quad (3)$$

where $P(x,t)$ is the probability density and $U'(x)$ is the derivative of the total potential.

At steady state, the probability current J becomes

$$J = -(U'_s(x) + f - v_0) P^s(x) + \frac{d}{dx} (T(x) P^s(x)), \quad (4)$$

The long-time steady-state current is given analytically by [14]

$$J = \frac{N}{D_1 D_2 + D_3 N}, \quad (5)$$

where the numerator is

$$N = 1 - \exp \left[\frac{L_0(f - v_0) - 2U_0/L_0}{2T_c} + \frac{L_0(f - v_0) + 2U_0/L_0}{2T_h} \right], \quad (6)$$

and the denominator components are

$$D_1 = \frac{e^{-\left(\frac{2U_0 + L_0(T_c + T_h)(f - v_0)}{2T_c T_h}\right)} (e^{U_0/T_c} - e^{L_0(f - v_0)/(2T_c)}) L_0}{2U_0 - L_0(f - v_0)} + \frac{\left(1 - e^{-\left(\frac{2U_0 + L_0(f - v_0)}{2T_h}\right)}\right) L_0}{2U_0 + L_0(f - v_0)}, \quad (7)$$

$$D_2 = \frac{e^{(2U_0 + L_0(f - v_0))/(2T_h)} (1 - e^{(-2U_0 + L_0(f - v_0))/(2T_c)}) L_0 T_c}{2U_0 - L_0(f - v_0)} + \frac{(1 - e^{(2U_0 + L_0(f - v_0))/(2T_h)}) L_0 T_h}{2U_0 + L_0(f - v_0)}, \quad (8)$$

$$D_3 = D_{31} + D_{32}, \quad (9)$$

with

$$D_{31} = \frac{L_0^2}{2(2U_0 + L_0(f - v_0))^2} \left[2 \left(1 - e^{-\left(\frac{2U_0 + L_0(f - v_0)}{2T_h}\right)}\right) T_h + 2U_0 + L_0(f - v_0) \right], \quad (10)$$

$$D_{32} = \frac{L_0^2}{2} \left[\frac{\Delta_1 T_c}{(2U_0 - L_0(f - v_0))^2 (-4U_0^2 + L_0^2(f - v_0)^2)} + \frac{\Delta_2 T_h}{(2U_0 - L_0(f - v_0)) (-4U_0^2 + L_0^2(f - v_0)^2)} \right], \quad (11)$$

where

$$\begin{aligned} \Delta_1 &= 1 - \exp \left(\frac{-2U_0 + L_0(f - v_0)}{2T_c} \right), \\ \Delta_2 &= 2 \exp \left(\frac{-2T_c U_0 - L_0(T_c + T_h)(f - v_0)}{2T_c T_h} \right) \left(1 - \exp \left(\frac{2U_0 + L_0(f - v_0)}{2T_h} \right) \right) \\ &\quad \left(\exp \left(\frac{U_0}{T_c} \right) - \exp \left(\frac{L_0(f - v_0)}{2T_c} \right) \right). \end{aligned} \quad (12)$$

Far from the quasistatic limit, the relationship between the steady-state current (or equivalently, the particle velocity) and the model parameters can be systematically examined. The contour plot in Fig. 2 illustrates how the average velocity of the hybrid Brownian motor depends on both the active propulsion strength v_0 and the potential barrier height U_0 . In general, the velocity steps up with v_0 which indicates that stronger self-propulsion enhances directed motion. However, the influence of U_0 is more nuanced. For passive transport ($v_0 = 0$), increasing U_0 initially enhances velocity due to the improved rectification of thermal fluctuations. However, beyond a certain point, further increases in U_0 suppress the motion because of the growing energetic barrier. This explains the local maximum along the $v_0 = 0$ axis observed in the figure. In the active regime ($v_0 > 0$), there exists a nontrivial interplay between active driving and potential barriers: at moderate U_0 , increasing v_0 results in

a sharp rise in velocity, reflecting a regime where activity and thermal rectification synergistically promote transport. On the other hand, at high U_0 , even strong self-propulsion becomes insufficient to overcome the steep barriers, and this leads to reduced net motion. Overall, these results highlight the dual and sometimes competing roles of thermal asymmetry and active propulsion in shaping transport characteristics.

Figure 3 depicts the regime in which the velocity or power output of the motor is maximized. In the figure, we plot the relationship between the potential barrier height U_0 and the propulsion velocity v_0 for fixed values of τ (fixed at 2, 3, 4, 5, 6, and 7 from top to bottom) while keeping $f = 0$. At these optimal values of U_0 and v_0 , although the efficiency is not necessarily maximized, the system operates at its maximum velocity or power output in this regime.

The total energy input per cycle consists of both pas-

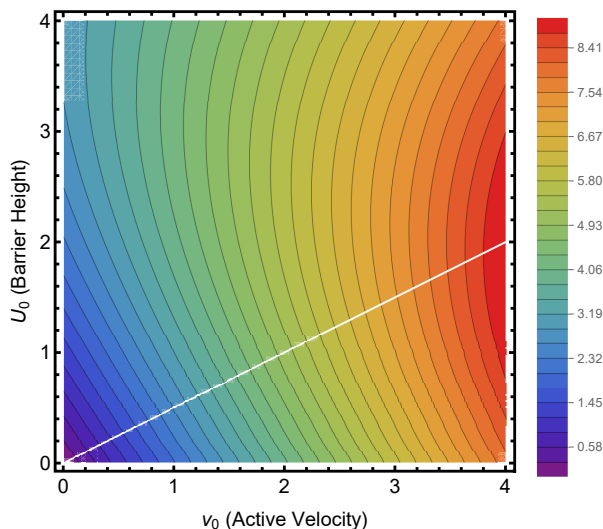


FIG. 2: Contour plot of particle velocity $v = L_0 J$ as a function of active velocity v_0 and barrier height U_0 . Parameters are fixed as $\tau = 2$ and $f = 0.0$.

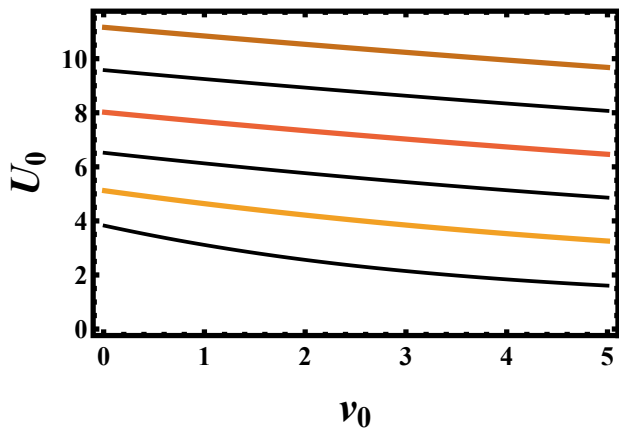


FIG. 3: Plot of U_0 vs v_0 where the velocity of the motor is maximum. The parameters are fixed as τ (fixed at 2, 3, 4, 5, 6, and 7 from top to bottom) and $f = 0$, with other relevant system parameters appropriately defined.

sive and active contributions. The minimum needed input energy required to cross the potential barrier so that the particle can move has a form

$$Q_1 = U_0 + \frac{fL_0}{2} + \frac{v_0 L_0}{2}. \quad (13)$$

Here, U_0 and $fL_0/2$ denote passive inputs due to potential and load, respectively. The expression $v_0 L_0/2$ denotes the energy input due to self-propulsion. At this point, we emphasize that Eq. (13) represents the minimum input energy required for the particle to complete one spatial cycle of ratchet potential. This energy comprises three distinct contributions. The potential bar-

rier height U_0 represents the energetic cost of overcoming a spatially periodic landscape. The term $fL_0/2$ accounts for the average work required to move the particle against the external load over half a cycle, and the term $v_0 L_0/2$ quantifies the effective energy consumption associated with the active propulsion force over the same distance. The appearance of the factor $1/2$ in both the load and propulsion terms reflects the symmetry of the ratchet potential and the average work over half of its period. Importantly, this expression corresponds to the minimal input energy requirement for directed transport.

We write the useful work output per cycle as

$$W = fL_0. \quad (14)$$

Thus, the efficiency of the hybrid Brownian motor can be written as

$$\eta = \frac{fL_0}{Q_1} = \frac{2fL_0}{2U_0 + fL_0 + v_0 L_0}. \quad (15)$$

In the quasistatic limit, the system approaches reversible dynamics, which corresponds to the condition where the steady-state current $J \rightarrow 0$. In the limit $J \rightarrow 0$, the stall force f_c at which the current is zero is given by

$$f_c = \frac{-2T_c U_0 + 2T_h U_0 + L_0 T_c v_0 + L_0 T_h v_0}{L_0(T_c + T_h)}. \quad (16)$$

Note that this critical force is obtained by setting the steady-state current $J = 0$ in Eq. (5), which corresponds to the quasistatic regime where the system approaches reversible states. Evaluating the efficiency at this quasistatic limit, one gets

$$\eta_{qs} = 1 - \frac{2T_c U_0}{2T_h U_0 + L_0(T_c + T_h)v_0}. \quad (17)$$

Surprisingly, in the limit $v_0 \rightarrow 0$, the particle behaves as a passive motor, and the quasistatic efficiency simplifies to

$$\eta_{qs}^{\text{passive}} = 1 - \frac{T_c}{T_h}, \quad (18)$$

which is the Carnot efficiency. In contrast, in the absence of a ratchet potential $U_0 \rightarrow 0$, the particle acts purely as an active motor and the efficiency becomes

$$\eta_{qs}^{\text{active}} = 1, \quad (19)$$

This shows that all the input energy is converted into useful work.

The quasistatic limit of the efficiency as a function of the model parameters can be examined using Eq. (17). Figure 4 shows the efficiency η of a hybrid Brownian motor as a function of the ratchet potential height U_0 and active propulsion velocity v_0 . The temperature was fixed as $\tau = 2$ ($\tau = 2$, $\eta_{qs} = 0.5$ for the passive motor). As expected, the efficiency increases with increasing active propulsion velocity v_0 , indicating that stronger

FIG. 4: Contour plot showing the efficiency η_{qs} of the hybrid Brownian motor as a function of the ratchet potential height U_0 and active propulsion velocity v_0 . The plot depicts how the efficiency depends on both the thermal asymmetry (represented by the temperatures T_h and T_c) and the active motion of the particle. The temperature parameters are fixed as $T_h = 2$ and $T_c = 1$. In the absence of active propulsion velocity v_0 , the efficiency at the quasistatic limit approaches $\eta_{qs} \rightarrow 0.5$ and this corresponds to the Carnot efficiency. The efficiency of the system approaches unity in the absence of ratchet potential. In intermediate regions (where both the passive and active forces contribute), the motor's efficiency ranges between the Carnot efficiency to one which indicates that the dual contribution of thermal rectification and self-propulsion.

self-propulsion enhances the directed motion of the particle. However, for large values of the ratchet potential height U_0 , the efficiency starts to decrease due to the higher energetic cost of overcoming the potential barriers. For moderate values of U_0 , the efficiency sharply increases with v_0 which reflects a regime where both active propulsion and thermal rectification synergistically improve particle transport. On the other hand, at very high values of U_0 , even strong self-propulsion cannot overcome the trapping effect of the potential, and this leads to a decrease in the velocity and efficiency. These findings highlight the dual role of thermal asymmetry and active forces in regulating the motion of particles, providing insights into the behavior of hybrid active-passive systems.

Figure 4 also depicts that (in the quasistatic limit), the efficiency of the system approaches unity in the absence of the ratchet potential, and the engine behaves as a chemically driven motor. When the active propulsion velocity v_0 is set to zero, the motor operating in a spatially varying temperature field transitions into a passive engine, and its efficiency asymptotically approaches the Carnot efficiency. For instance, when the temperature parameters are fixed at $T_h = 2$ and $T_c = 1$, the efficiency at the quasistatic limit approaches $\eta_{qs} \rightarrow 0.5$,

which corresponds to the Carnot efficiency. In intermediate regions (where both the passive and active forces contribute), the motor's efficiency ranges between the Carnot efficiency to one which indicates that the dual contribution of thermal rectification and self-propulsion. This behavior demonstrates the transition from purely passive to hybrid active-passive operation, with efficiency spanning from the fundamental thermodynamic limit of Carnot to the idealized efficiency of a chemically driven engine.

We now investigate the degree of irreversibility by examining the relationship between the entropy production rate \dot{e}_p , the entropy extraction rate \dot{h}_d , and the efficiency of the system. The non-equilibrium Gibbs entropy [44–47]

$$S(t) = - \int P(x, t) \ln P(x, t) dx \quad (20)$$

is a fundamental relation in statistical mechanics that helps describe the entropy of systems that are far from equilibrium. The entropy change is given by [25]

$$\frac{dS(t)}{dt} = \dot{e}_p - \dot{h}_d \quad (21)$$

where \dot{e}_p is the entropy production rate and \dot{h}_d is the entropy dissipation rate, defined as

$$\dot{e}_p = \int \frac{J^2}{P(x, t)T(x)} dx, \quad (22)$$

$$\dot{h}_d = \int \left(J \frac{U'(x)}{T(x)} + J \frac{T'(x)}{2T(x)} \right) dx. \quad (23)$$

Unlike the isothermal case, the term $J \frac{T'(x)}{2T(x)}$ introduces an additional contribution to the entropy dissipation. At the steady state ($\frac{dS(t)}{dt} = 0$), it follows that $\dot{e}_p = \dot{h}_d > 0$. Because the current J is independent of position, after some algebraic manipulations, we obtain the following expression for the entropy extraction rate:

$$\dot{e}_p = \dot{h}_d = \frac{JL_0}{2} \left[\frac{\left(\frac{2U_0}{L_0} + (f - v_0) \right)}{T_h} + \frac{\left(-\frac{2U_0}{L_0} + (f - v_0) \right)}{T_c} \right]. \quad (24)$$

At the quasistatic limit, when $J \rightarrow 0$, the entropy extraction rate $\dot{h}_d \rightarrow 0$ which shows that the efficiency of the system approaches the Carnot efficiency.

In the absence of the ratchet potential ($U_0 \rightarrow 0$), the equation simplifies to

$$\dot{e}_p = \dot{h}_d = \frac{(f - v_0)^2}{T_c}, \quad (25)$$

which shows that the entropy production rate is directly proportional to the square of the external force $f - v_0$ and inversely proportional to the cold bath temperature

T_c . In the case where $f \rightarrow v_0$, the expression becomes zero, and in this regime, the efficiency of the active motor approaches one.

In conclusion, in this work, we developed and analyzed a hybrid Brownian motor model that combines self-propulsion with thermally driven transport in a ratchet potential under a piecewise constant temperature profile. By introducing an effective driving force $f - v_0$, we unified the active and passive transport mechanisms within a common framework. We derived exact expressions for the steady-state current and evaluated the energetic efficiency in both the active and passive limits. Our results show that the efficiency approaches unity when the ratchet potential is zero, which is consistent with the behavior of a chemically driven active motor. On the other hand, in the passive limit ($v_0 \rightarrow 0$), the efficiency reaches the Carnot bound, which indicates reversible thermo-

dynamics under spatial temperature asymmetry. These findings highlight the rich and tunable behavior of hybrid microscopic engines and open new possibilities for optimizing transport and energy conversion at small scales.

Acknowledgements

I would also like to thank Mulu Zebene and Asfaw Taye for the constant encouragement.

Data Availability Statement

Data sharing is not applicable to this article as no data sets were generated or analyzed during the current study.

-
- [1] P. Hänggi, F. Marchesoni, and F. Nori, *Ann. Phys. (Leipzig)* **14**, 51 (2005).
- [2] P. Hänggi and F. Marchesoni, *Rev. Mod. Phys.* **81**, 387 (2009).
- [3] T. Hondou and K. Sekimoto, *Phys. Rev. E* **62**, 6021 (2000).
- [4] A.G. Marin and J.M. Sancho, *Phys. Rev. E* **74**, 062102 (2006).
- [5] N. Li, F. Zhan, P. Hänggi, and B. Li, *Phys. Rev. E* **80**, 011125 (2009).
- [6] N. Li, P. Hänggi, and B. Li, *Europhysics Letters* **84**, 40009 (2008).
- [7] F. Zhan, N. Li, S. Kohler, and P. Hänggi, *Phys. Rev. E* **80**, 061115 (2009).
- [8] M. Büttiker, *Z. Phys. B* **68**, 161 (1987).
- [9] N.G. van Kampen, *IBM J. Res. Dev.* **32**, 107 (1988).
- [10] R. Landauer, *J. Stat. Phys.* **53**, 233 (1988).
- [11] R. Landauer, *Phys. Rev. A* **12**, 636 (1975).
- [12] R. Landauer, *Helv. Phys. Acta* **56**, 847 (1983).
- [13] P. Reimann, R. Bartussek, R. Häussler, and P. Hänggi, *Phys. Lett. A* **215**, 26 (1996).
- [14] M. Asfaw and M. Bekele, *Eur. Phys. J. B* **38**, 457 (2004).
- [15] M. Asfaw and M. Bekele, *Phys. Rev. E* **72**, 056109 (2005).
- [16] M. Asfaw and M. Bekele, *Physica A* **384**, 346 (2007).
- [17] M. Matsuo and S. Sasa, *Physica A* **276**, 188 (1999).
- [18] I. Derényi and R.D. Astumian, *Phys. Rev. E* **59**, R6219 (1999).
- [19] I. Derényi, M. Bier, and R.D. Astumian, *Phys. Rev. Lett* **83**, 903 (1999).
- [20] J.M. Sancho, M. S. Miguel, and D. Dürr, *J. Stat. Phys.* **28**, 291 (1982).
- [21] B.Q. Ai, H.Z. Xie, D.H. Wen, X.M. Liu, and L.G. Liu, *Eur. Phys. J. B* **48**, 101 (2005).
- [22] M. Asfaw, *Eur. Phys. J. B* **86**, 189 (2013).
- [23] F. L. Curzon and B. Ahlborn, *Am. J. Phys.* **43**, 22 (1975).
- [24] M. Asfaw, *Phys. Rev. E* **89**, 012143 (2014).
- [25] M. A. Taye, *Phys. Rev. E* **94**, 032111 (2016).
- [26] M. A. Taye, *Phys. Rev. E* **101**, 012131 (2020).
- [27] M. A. Taye, *Phys. Rev. E* **110**, 054105 (2024).
- [28] M. A. Taye, *Phys. Rev. E* **105**, 054126 (2022).
- [29] O. Reynolds, *Phil Trans Royal Soc London* **177**, 157 ((1886).
- [30] M. Asfaw and S. F. Duki, *Eur. Phys. J. B* **88**, 322 (2015).
- [31] D. Breoni, M. Schmiedeberg, and H. Löwen, *Phys. Rev. E* **102**, 062604 (2020). DOI: 10.1103/PhysRevE.102.062604
- [32] A. K. Omar, K. Klymko, T. GrandPre, and P. L. Geissler, *Phys. Rev. Lett.* **126**, 088002 (2021). DOI: 10.1103/PhysRevLett.126.088002
- [33] L. Caprini and U. M. B. Marconi, *Soft Matter* **17**, 4109 (2021). DOI: 10.1039/D0SM02273J
- [34] J. Bickmann and R. Wittkowski, *J. Phys.: Condens. Matter* **32**, 214001 (2020). DOI: 10.1088/1361-648X/ab5e0e
- [35] M. Su and B. Lindner, *Eur. Phys. J. E* **46**, 22 (2023). DOI: 10.1140/epje/s10189-023-00283-w
- [36] S. Bröker, M. te Vrugt, and R. Wittkowski, *Commun. Phys.* **7**, 238 (2024). DOI: 10.1038/s42005-024-01674-x
- [37] M. Sanoria, R. Chelakkot, and A. Nandi, *Soft Matter* **20**, 9184 (2024). DOI: 10.1039/D4SM00981A
- [38] T. Knippenberg, A. Jayaram, T. Speck, and C. Bechinger, *Phys. Rev. Lett.* **133**, 048301 (2024). DOI: 10.1103/PhysRevLett.133.048301
- [39] Z. Liu and M. Dijkstra, *Soft Matter* **21**, 1234 (2025). DOI: 10.1039/D4SM01270D
- [40] M. Wiśniewski and J. Spiechowicz, *Phys. Rev. E* **111**, 024130 (2025). DOI: 10.1103/PhysRevE.111.024130
- [41] K. Sasaki, R. Kanada, and S. Amari, *J. Phys. Soc. Jpn.* **76**, 023003 (2007).
- [42] K. H. Kim and H. Qian, *Phil. Trans. R. Soc. A* **371**, 20120059 (2013).
- [43] S. Nath, *Biophys. Chem.* **219**, 69 (2016).
- [44] T. Tomé and M. J. de Oliveira, *Phys. Rev. Lett.* **108**, 020601 (2012).
- [45] J. Schnakenberg, *Rev. Mod. Phys.* **48**, 571 (1976).
- [46] U. Seifert, *Phys. Rev. Lett.* **95**, 040602 (2005).
- [47] T. Tomé, *Braz. J. Phys.* **36**, 1285 (2006).